
Improving Adversarial Attacks on Latent Diffusion Model

Boyang Zheng^{*1} Chumeng Liang^{*2} Xiaoyu Wu¹ Yan Liu²

Abstract

Adversarial attacks on Latent Diffusion Model (LDM), the state-of-the-art image generative model, have been adopted as effective protection against malicious finetuning of LDM on unauthorized images. We show that these attacks add an extra error to the score function of adversarial examples predicted by LDM. LDM finetuned on these adversarial examples learns to lower the error by a bias, from which the model is attacked and predicts the score function with biases.

Based on the dynamics, we propose to improve the adversarial attack on LDM by Attacking with Consistent score-function Errors (ACE). ACE unifies the pattern of the extra error added to the predicted score function. This induces the finetuned LDM to learn the same pattern as a bias in predicting the score function. We then introduce a well-crafted pattern to improve the attack. Our method outperforms state-of-the-art methods in adversarial attacks on LDM.

1. Introduction

Latent Diffusion Model (LDM) (Rombach et al., 2022; Podell et al., 2023) has achieved state-of-the-art performance in image synthesis. LDM steps Gaussian noise to examples gradually with the score function predicted by the model. Combining the sampling architecture of Denoising Diffusion Models (DDMs) (Sohl-Dickstein et al., 2015; Song & Ermon, 2019; Ho et al., 2020; Song et al., 2020) and the latent representation space built by VQGAN (Esser et al., 2021), LDM is able to generate high-resolution images guided by text. A significant breakthrough of LDM is its few-shot generation, to generate images with certain contents by finetuning on several samples (Meng et al., 2021; Gal et al., 2022; Ruiz et al., 2023; Ye et al., 2023). This yet raises the copyright and ethical concerns (Fan et al., 2023; Chen et al., 2023; Wang et al., 2023b), while malicious ones

may make profits from copying unauthorized artworks with few-shot generation pipelines of LDM.

Recognizing the need, adversarial attacks on LDM were born as countermeasures (Salman et al., 2023; Liang et al., 2023; Shan et al., 2023a; Van Le et al., 2023; Shan et al., 2023b). These attacks add tiny perturbations to images and transfer them to adversarial examples. LDM finetuned on these adversarial examples produces sampled images with chaotic patterns, which makes the images unusable. This prevents unauthorized copying of the images. Applications based on these adversarial attacks (Shan et al., 2023a; Liang & Wu, 2023; Shan et al., 2023b) safeguard personal images from being used in LDM-empowered few-shot generation.

In this paper, we reveal the dynamics of adversarial attacks on LDM. As demonstrated in Figure 2, adversarial examples for LDM add an extra error term to the predicted score function of adversarial examples. This extra error is mitigated in the LDM finetuned on adversarial examples by a learned *reverse bias*. Here, *reverse bias* means the bias has a reverse direction to the error. Both extra errors and reverse biases do not contain useful semantics. Affected by reverse biases, LDM includes a sampling bias, accumulating considerable errors on the sample.

We exploit this dynamics to improve adversarial attacks on LDM. We find that by making extra errors for different adversarial consistent with one single pattern, the sampling bias also shares this pattern. This allows us to specify and optimize the pattern of the sampling bias. We denote this method by Attacking with Consistent score-function Errors (ACE). We then propose a desirable pattern for ACE. Combining two improvements, ACE outperforms existing adversarial attacks on LDM in countering finetuning-based few-shot generation.

The contributions of this paper are two-fold. First, we reveal the dynamics of adversarial attacks on LDM, which provides a novel view of the interpretation and performance analysis of these adversarial attacks. Second, we propose Attack with Consistent Error (ACE), an improved adversarial attack on LDM. ACE outperforms existing adversarial attacks on LDM in disrupting the finetuning of LDM and serves as a practical tool in protecting images from being used in unauthorized artwork copying or malicious image faking empowered by LDM.

^{*}Equal contribution ¹Shanghai Jiao Tong University, Shanghai, China ²University of Southern California, Los Angeles, USA. Correspondence to: Chumeng Liang <caradryan2022@gmail.com>.

2. Background

Latent Diffusion Model Latent Diffusion Model (Rombach et al., 2022) is a DDM that samples in a latent representation space of images built by training an encoder and a decoder of VQGAN (Esser et al., 2021). Specifically, the encoder encodes an image x to a latent representation z and the decoder decodes z back the the image: $\tilde{x} = \mathcal{D}(z) = \mathcal{D}(\mathcal{E}(x))$. Having $x \in \mathbb{R}^{H \times W \times C}$ and $z \in \mathbb{R}^{h \times w \times c}$, the encoder downsamples x by a factor $f = \frac{H}{h} = \frac{W}{w} = 2^m, m \in \mathbb{N}$. The forward process of DDM perturbs the latent representation step by step to Gaussian noise. Then, a parameterized score-function estimator s_θ learns to gradually denoise the Gaussian noise to plausible latent representations, called the reverse process. These two processes are interpreted by a pair of forward-time and reverse-time SDE (Anderson, 1982; Song et al., 2020) in the latent representation space:

$$\begin{aligned} dz &= \mathbf{f}(z, t)dt + g(t)d\mathbf{w} \\ dz &= [\mathbf{f}(z, t) - g^2(t)\nabla_z \log p_t(z)]dt + g(t)d\bar{\mathbf{w}} \end{aligned} \quad (1)$$

where \mathbf{w} and $\bar{\mathbf{w}}$ are standard Wiener processes when time flows from 0 to T and backwards, and dt are infinitesimal timesteps (Song et al., 2020). LDM instantiates $\mathbf{f}(z, t)$ and $g(t)$ as $-\frac{1}{2}\beta(t)$ and $\sqrt{\beta(t)}$ where $\beta(t) = \beta_0 + t \cdot (\beta_T - \beta_0)$, following linear noise schedule (Ho et al., 2020).

LDM is trained by minimizing the **score-function error**, the difference between predicted score-function $s_\theta(z, t)$ by neural network θ and the ground truth score function $\nabla_z \log p_t(z)$, since the score function is the only unknown term in Equation 1. The training objective is given by:

$$\begin{aligned} \min_{\theta} \mathbb{E}_t \mathbb{E}_{z(t)|z(0)} \left\| \underbrace{s_\theta(z(t), t) - \nabla_{z(t)} \log p_t(z(t)|z(0))}_{\epsilon_\theta(z(t), t): \text{score-function error}} \right\|_2^2 \\ \text{where } z'(0) = \mathcal{E}(x) \end{aligned} \quad (2)$$

Adversarial Attacks on Latent Diffusion Model Adversarial attacks on Latent Diffusion Model (Salman et al., 2023; Liang et al., 2023; Shan et al., 2023a; Liang & Wu, 2023; Van Le et al., 2023; Zhao et al., 2023; Xue et al., 2023) generate adversarial examples by adding tiny adversarial perturbations to clean images. The generated adversarial examples are unusable for finetuning LDM, by which these attacks serve as powerful tools to protect personal images from being used in finetuning LDM.

Generally, adversarial attacks on LDM raise the training loss of LDM (Liang et al., 2023; Van Le et al., 2023; Zhao et al., 2023; Xue et al., 2023) or make the example semantically similar to other examples with different contents (Salman et al., 2023; Shan et al., 2023a; Liang & Wu, 2023). One commonality of these attacks is that they generate adversarial examples on the backbone LDM (the base model of finetuning) while the adversarial examples dramatically degrade the performance of the LDM finetuned on them.

This is very different from adversarial attacks on classification models (Szegedy et al., 2013; Goodfellow et al., 2014; Madry et al., 2017; Carlini & Wagner, 2017), for adversarial training (Goodfellow et al., 2014) (training models on adversarial examples) enhances robustness of models at only little cost of overall performance. The mechanism why adversarial attacks on LDM can disrupt finetuning by raising training loss of the backbone LDM is unknown.

Notation The rest of the paper uses the following notation:

x and $z(t)$: clean image and its latent representations.

x' and $z'(t)$: corresponding adversarial example and latent representations. $\|x' - x\| \leq \zeta$ with adversarial budget ζ .

$\mathcal{E}(\cdot)$ and $\mathcal{D}(\cdot)$: The encoder and decoder of LDM

θ : the backbone LDM.

θ^* : the LDM finetuned on clean images.

ϕ : the LDM finetuned on adversarial examples

3. Dynamics of Adversarial Attacks on LDM

In this section, we demonstrate the dynamics how adversarial attacks on LDM disturb the finetuning of LDM. Section 3.1 shows that attacks add an extra score-function error to the adversarial example. Section 3.2 discusses how these errors disturb the finetuning. Section 3.3 summarizes the dynamics.

3.1. Score-function Errors of Adversarial Examples

We start from examining the score-function errors (defined in Equation 2) of both clean images and adversarial examples on the backbone LDM θ (without finetuning), for existing adversarial attacks on LDM target on maximizing score-function error directly or indirectly.

For a clean image x , we have $z(0) = \mathcal{E}(x)$ and use Equation 1 to sample $z(t)$ given $z(0)$. The score-function error $\epsilon_\theta(z(t), t)$ only has one component ϵ_{inh} :

$$\mathbb{E}_{z(t)|z(0)} \epsilon_\theta(z(t), t) = \epsilon_{inh} \quad (3)$$

Here, ϵ_{inh} is the inherent score-function error that originates from the fact that LDM cannot perfectly predict the score function of every clean image. For the adversarial example x' corresponding to x , we obtain $z'(0)$ and $z'(t)$ in a similar way. Its score-function error $\epsilon_\theta(z'(t), t)$ consists of two components ϵ_{int} and ϵ_{adv} :

$$\begin{aligned} \mathbb{E}_{z'(t)|z'(0)} \epsilon_\theta(z'(t), t) &= \epsilon_{inh} + \epsilon_{adv} \\ &= \mathbb{E}_{z(t)|z(0)} \epsilon_\theta(z(t), t) + \epsilon_{adv} \end{aligned} \quad (4)$$

Here, ϵ_{inh} is the inherent score-function error succeeded from the clean image x . ϵ_{adv} is the extra score-function error brought by adversarial attacks.

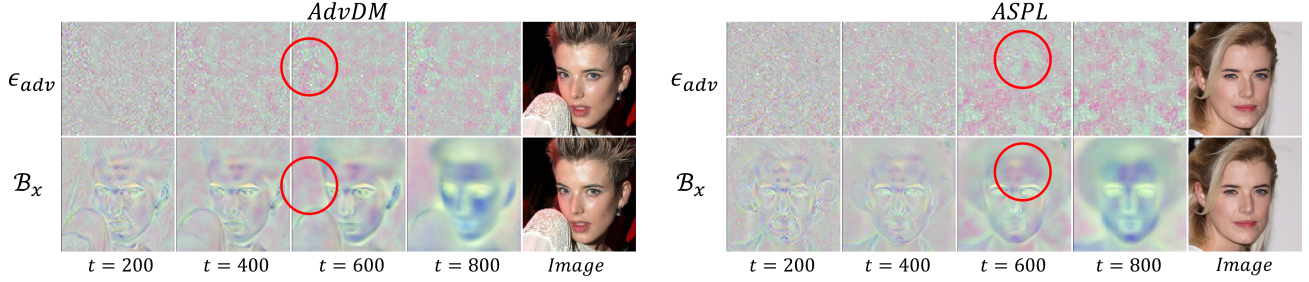


Figure 1. The comparison of ϵ_{adv} and \mathcal{B}_x for AdvDM (Liang et al., 2023) and ASPL (Van Le et al., 2023), two existing adversarial attacks on LDM. We have $\epsilon_{adv}, \mathcal{B}_x \in \mathbb{R}^{64 \times 64 \times 4}$. We visualize them as images with 4 channels and complementary colors mean two pixel are reverse to each other. Red cycles note distinguished districts that \mathcal{B}_x reverses ϵ_{adv} . Visualization details are given in Appendix A.5

3.2. Reverse Bias in Adversarial Finetuning

Few-shot generation pipelines of LDM, including textual inversion (Gal et al., 2022), Dreambooth (Ruiz et al., 2023), and LoRA (Hu et al., 2021), are methods of Parameter-Efficient Fine-Tuning (PEFT) (Devlin et al., 2018). Finetuning LDM with these methods on adversarial examples x^* learns to lower the score-function error.

In this part, we mainly consider an LDM θ , which is used as the backbone model in finetuning, and an LDM ϕ , which is finetuned on the adversarial examples.

Consider two components of adversarial examples' score-function error given by Equation 4. Since the LDM ϕ is finetuned to lower these two components for adversarial example x' , the finetuned score-function error for adversarial example x' can be given by:

$$\mathbb{E}_{z'(t)|z'(0)} \epsilon_\phi(z'(t), t) = (1 - \lambda_{inh}) \epsilon_{inh} + (1 - \lambda_{adv}) \epsilon_{adv} \quad (5)$$

Here, $\lambda_{inh}, \lambda_{adv} \in (0, 1)^{h \times w \times c}$ are two factors that illustrate the finetuning effect in lowering two error components.

We know that $s_\theta(z) = \nabla_z \log p_t(z) + \epsilon_\theta(z, t)$ and that $\nabla_z \log p_t(z)$ is the constant ground truth. Therefore, we compute the difference between predicted score functions by the difference between score-function errors:

$$\begin{aligned} & \mathbb{E}_{z'(t)|z'(0)} [s_\phi(z'(t), t) - s_\theta(z'(t), t)] \\ &= \mathbb{E}_{z'(t)|z'(0)} [\epsilon_\phi(z'(t), t) - \epsilon_\theta(z'(t), t)] \quad (6) \\ &= -\lambda_{inh} \epsilon_{inh} - \lambda_{adv} \epsilon_{adv} \end{aligned}$$

The predicted score functions for *adversarial example* x' of the finetuned LDM ϕ is then given as follows:

$$\begin{aligned} & \mathbb{E}_{z'(t)|z'(0)} [s_\phi(z'(t), t)] \\ &= \mathbb{E}_{z'(t)|z'(0)} [s_\theta(z'(t), t)] - \underbrace{\lambda_{inh} \epsilon_{inh} - \lambda_{adv} \epsilon_{adv}}_{\mathcal{B}_x(t): \text{reverse bias}} \quad (7) \end{aligned}$$

There are two new bias terms reverse to two components of the score-function error in the finetuned predicted score function. The first term $-\lambda_{inh} \epsilon_{inh}$ lowers the inherent score-function error. This term contains the semantic of

images and improves the sample quality of the finetuned LDM, which is expected in the normal finetuning.

The second term $-\lambda_{adv} \epsilon_{adv}$, however, lowers the extra score-function error ϵ_{adv} brought by adversarial attacks. Because its direction is reverse to the extra error ϵ_{adv} , we call it a **reverse bias**. Since ϵ_{adv} does not contain image semantics, LDM learns no useful semantics from lowering ϵ_{adv} by the reverse bias. In fact, LDM even learns general **sampling biases** that contain some chaotic patterns when predicting score functions for non-adversarial inputs, which is suggested by the chaotic pattern of output images of the finetuned LDM under existing attacks (Liang et al., 2023; Van Le et al., 2023). This is the reason why adversarial attacks on LDM can disturb the finetuning of LDM. To validate the existence of the reverse bias, we compute the true bias $\mathcal{B}_x(t)$ and show that it reverses ϵ_{adv} . From Equation 6, we know that $\mathcal{B}_x(t)$ can be expressed by:

$$\mathcal{B}_x(t) = \mathbb{E}_{z'(t)} [\epsilon_\phi(z'(t), t) - \epsilon_\theta(z'(t), t)] + \lambda_{inh} \epsilon_{inh} \quad (8)$$

where $\lambda_{inh} \epsilon_{inh}$ is unknown. However, $\lambda_{inh} \epsilon_{inh}$ is the bias that lowers the inherent error ϵ_{inh} , which also appears in the finetuning on clean examples. Hence, we have the following estimate with an LDM θ^* finetuned on clean examples:

$$\mathbb{E}_{z(t)} \epsilon_{\theta^*}(z(t), t) \approx (1 - \lambda_{inh}) \epsilon_{inh} \quad (9)$$

This is a rough estimation with systematic errors, for the finetuning factor λ_{inh} can be very different in the clean finetuning on θ^* and the adversarial finetuning on ϕ . Combining Equation 3, 8, and 9, we have $\mathcal{B}_x(t)$ as follows:

$$\begin{aligned} \mathcal{B}_x(t) &= \mathbb{E}_{z'(t)} [\epsilon_\phi(z'(t), t) - \epsilon_\theta(z'(t), t)] \\ &\quad - \mathbb{E}_{z(t)} [\epsilon_{\theta^*}(z(t), t) - \epsilon_\theta(z(t), t)] \quad (10) \end{aligned}$$

ϵ_{adv} is straight-forward to obtain with Equation 4:

$$\epsilon_{adv} = \mathbb{E}_{z'(t)} \epsilon_\theta(z'(t), t) - \mathbb{E}_{z(t)} \epsilon_\theta(z(t), t) \quad (11)$$

Figure 1 visualizes the comparison of the estimated $\mathcal{B}_x(t)$ and ϵ_{adv} for two existing adversarial attacks, AdvDM (Liang et al., 2023) and ASPL (Van Le et al., 2023).

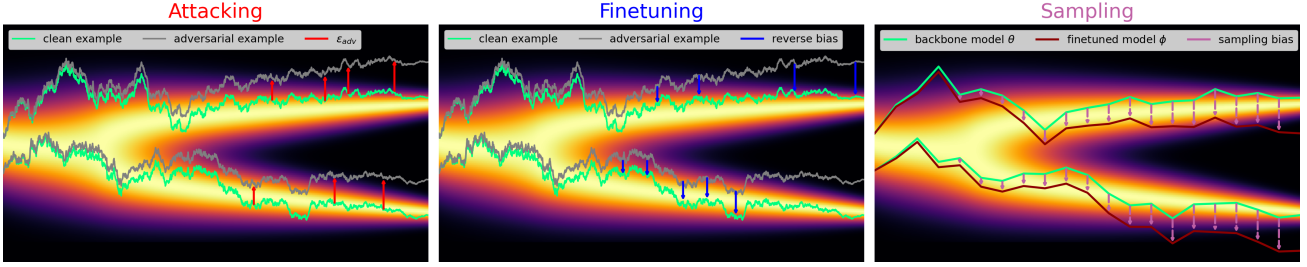


Figure 2. Dynamics of adversarial attacks on LDM. **Attacking** is conducted by the owner of the image while malicious ones try to mimic the image by **Finetuning** and **Sampling**. **Attacking** generates adversarial examples with extra score-function error ϵ_{adv} for the backbone LDM θ . **Finetuning** mitigates ϵ_{adv} by reverse bias \mathcal{B}_x . Different \mathcal{B}_x jointly impact **Sampling** by introducing a sampling bias \mathcal{B}_{spl} when predicting score functions for non-adversarial inputs, which accumulates to considerable errors on the sampled example.

It shows that $\mathcal{B}_x(t)$ and ϵ_{adv} are reversal to each other in some districts. Due to the systematic error in Equation 9, this result is expected. We also compute the cosine similarity between $\mathcal{B}_x(t)$ and ϵ_{adv} over different images, whose average is -0.205 and -0.370, respectively. Both qualitative and quantitative results indicate that there is a reversal correlation between the true bias $\mathcal{B}_x(t)$ and the extra error ϵ_{adv} .

3.3. Summary

The dynamic of ϵ_{adv} and the reverse bias explains how adversarial attacks on LDM disrupt finetuning. As demonstrated in Figure 2, adversarial examples generated by **Attacking** have an extra score-function error ϵ_{adv} . In **Finetuning**, the finetuned LDM ϕ mitigates ϵ_{adv} by a reverse bias \mathcal{B}_x . Since ϵ_{adv} does not contain normal image semantics, LDM only learns a meaningless or even chaotic sampling bias from mitigating ϵ_{adv} by \mathcal{B}_x . The sampling bias appears even when inputs are not adversarial. This bias finally accumulates to considerable errors over timesteps in the **Sampling**.

One observation is that **patterns** of extra errors ϵ_{adv} in existing adversarial attacks vary for different images. Here, *pattern* means the value distribution over $\mathbb{R}^{h \times w \times c}$. This shows that reverse biases \mathcal{B}_x also vary for different images. Due to the black box of neural networks, we do not know how these different reverse biases yield the sampling bias, thus being unable to specify and optimize the pattern of the sampling bias. Section 4 proposes a solution to this problem.

4. Improved Adversarial Attack on LDM by Attacking with Consistent Errors

Section 4 mentions that different reverse biases from different adversarial examples work jointly to bias the sampling of the finetuned LDM in existing attacks. Because errors ϵ_{adv} and their reverse biases \mathcal{B}_x diverse, we cannot specify and optimize the sampling bias. One intuitive idea is, *can*

we specify the sampling bias by making all ϵ_{adv} consistent with one single pattern?

The idea is straight-forward. If we make all ϵ_{adv} share the same pattern, the finetuned LDM will learn to lower errors with this single pattern with different inputs. Empirically, this is likely to lead to overfitting, that the finetuned LDM believes the pattern should be a constant bias to the predicted score function. This allows us to specify the sampling bias by specifying the shared pattern of ϵ_{adv} .

4.1. Attacking with Consistent Errors

Inspired by this idea, we design a new objective function to adversarially Attack LDM with Consistent Errors (ACE).

$$\max_{x'} \mathbb{E}_t \mathbb{E}_{z'(t)|z'(0)} \|s_\theta(z'(t), t) - \mathcal{T}\|_2^2 \quad (12)$$

where $z'(0) = \mathcal{E}(x')$, $\|x' - x\| \leq \zeta$

The objective pushes the predicted score function to an target $\mathcal{T} \in \mathbb{R}^{h \times w \times c}$. Empirically, we find that this objective function makes the error ϵ_{adv} for *different adversarial examples* share one pattern $\mathcal{G}(\mathcal{T})$, which only depends on the target \mathcal{T} . Their corresponding reverse bias also have the common pattern within.

The question is, will this shared pattern of ϵ_{adv} appear in the sampling bias? We give an affirmative answer by experimentally comparing ϵ_{adv} and the sampling bias \mathcal{B}_{spl} .

ϵ_{adv} can be obtained by Equation 11. Hence, we focus on computing the sampling bias \mathcal{B}_{spl} . The sampling bias is the difference between the predicted and ground truth score function. However, the ground truth score function is not tractable in the real sampling. For this reason, we cannot compute the sampling bias in the real sampling.

Instead, we select images which are out of the finetuning dataset but describe the same identity as the dataset. We sample $z(t)$ based on these images with Equation 1. For the predicted score function, we use such $z(t)$ as inputs and do the prediction with LDM ϕ , which is finetuned on adversarial examples by ACE. The ground truth score func-

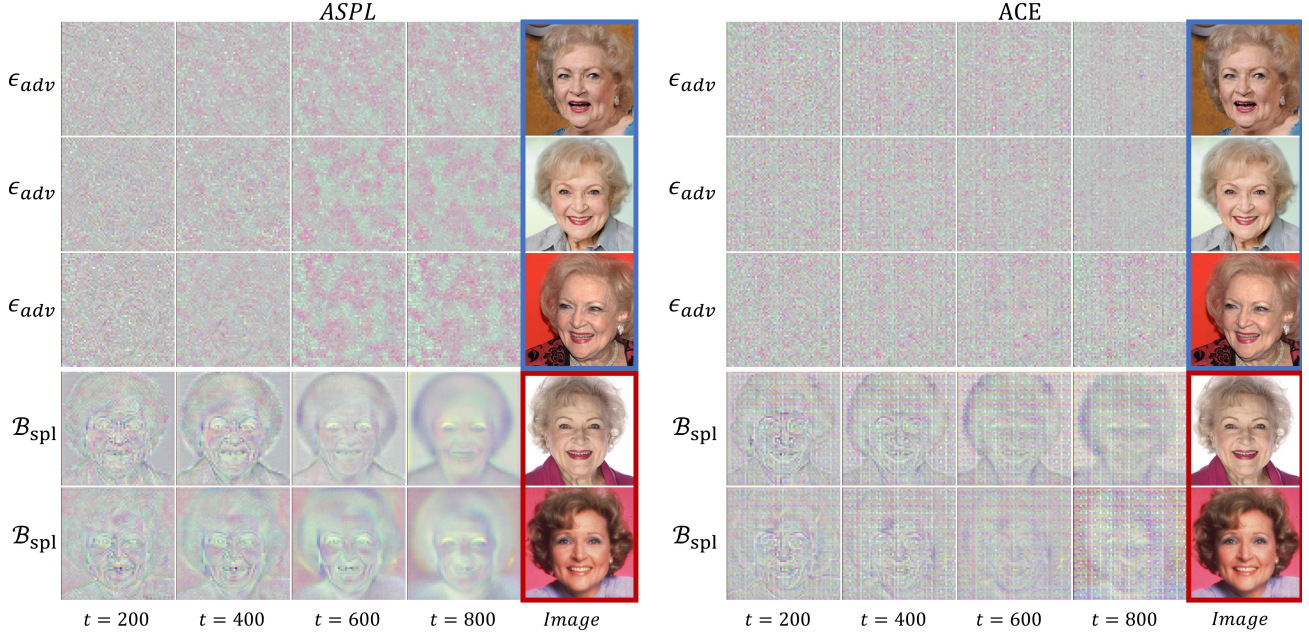


Figure 3. Comparison between ϵ_{adv} and \mathcal{B}_{spl} of ASPL (Van Le et al., 2023) and ACE. Images in the blue frame are adversarial examples covered by the finetuning dataset. We compute their extra errors ϵ_{adv} . Images in the red frame are clean images out of the dataset. We use their $z(t)$ to compute the sampling bias \mathcal{B}_{spl} . We have $\epsilon_{adv}, \mathcal{B}_{spl} \in \mathbb{R}^{64 \times 64 \times 4}$. We visualize them as images with 4 channels and complementary colors mean two pixel are reverse to each other. There is strong pattern correlation between ϵ_{adv} and \mathcal{B}_{spl} in ACE.

tion is given by the Gaussian noise added to $z(t)$. This is a simulation of one sampling step. The only difference (and advantage) is that we know the ground truth score function. Finally, we can compute the sampling bias as follows:

$$\mathcal{B}_{spl}(t) = \mathbb{E}_{z(t)|z(0)}[s_\phi(z(t), t) - \nabla_{z(t)} \log p_t(z(t)|z(0))] \quad (13)$$

We omit the dependency on $z(t)$ for convenience.

We are interested in to what extent the sampling bias $\mathcal{B}_{spl}(t)$ shares the pattern with the extra error ϵ_{adv} in practice. Hence, we visualize extra errors ϵ_{adv} for different adversarial examples and the sampling bias $\mathcal{B}_{spl}(t)$ for ASPL (Van Le et al., 2023) and ACE in Figure 3. There is no visible similarity between ϵ_{adv} and $\mathcal{B}_{spl}(t)$ in ASPL. By contrast, sampling biases in ACE show strong pattern similarity with ϵ_{adv} (different ϵ_{adv} are also similar). Two variables share the pattern with vertical stripes. We also compute the cosine similarity between ϵ_{adv} and \mathcal{B}_{spl} for existing attacks and ACE. Results in Table 4 shows that there is pattern similarity between ϵ_{adv} and \mathcal{B}_{spl} in ACE, while such similarity is absent in existing attacks.

Therefore, we can decompose the sampling bias into two components: one with the shared pattern $G(\mathcal{T})$ and the

other independent from $G(\mathcal{T})$. Let $\mathcal{B}_{inh}(t)$ be the independent component. We can estimate $\mathcal{B}_{spl}(t)$ as follows:

$$\mathcal{B}_{spl}(t) \approx \gamma_{spl}(t)G(\mathcal{T}) + \mathcal{B}_{inh}(t) \quad (14)$$

where $\gamma_{spl}(t)$ is approximately a scalar discounted factor and $G(\mathcal{T}) \in \mathbb{R}^{h \times w \times c}$ is the shared pattern. With Equation 14 and the sampling process defined in Equation 1, we can express the sampling error η_{spl} accumulated on the sampled $z(0)$:

$$\begin{aligned} \eta_{spl} &= \sum_{t=1}^T \beta(t)\mathcal{B}_{spl}(t) \\ &\approx G(\mathcal{T}) \sum_{t=1}^T \beta(t)\gamma_{spl}(t) + \sum_{t=1}^T \beta(t)\mathcal{B}_{inh}(t) \end{aligned} \quad (15)$$

The sampling error η_{spl} also includes a component with the shared pattern $G(\mathcal{T})$. This indicates that **we can partially specify and then optimize the pattern of the sampling error by changing \mathcal{T} in ACE**. This is the main advantage of ACE.

4.2. Pattern Selection

The motivation to specify the sampling error is to optimize its pattern so that it further degrades the sample quality. In Section 4.1, we show that ACE is capable to specify the sampling error by tuning \mathcal{T} in Equation 12. We then explore what kind of targets \mathcal{T} can most degrade the sampling quality. Empirically, we find that the latent representation

Method	Cosine SIM
AntiDB	-0.009372
AdvDM	-0.004139
ACE	-0.304395

Figure 4. Cosine similarity between ϵ_{Adv} and \mathcal{B}_{spl} .

Algorithm 1 Attacking with Consistent Errors (ACE)

```

1: Input: Image  $x$ , LDM  $\theta$ , learning rates  $\alpha, \gamma$ , epoch
   numbers  $N, M, K$ , budget  $\zeta$ , loss function  $\mathcal{L}_{LDM}$  in
   Equation 2, objective function  $J$  in Equation 12 (ACE)
   & Equation 16 (ACE+).
2: Output: Adversarial example  $x'$ 
3: Initialize  $x' \leftarrow x$ .
4: for  $n$  from 1 to  $N$  do
5:   for  $m$  from 1 to  $M$  do
6:      $\theta \leftarrow \theta - \gamma \nabla_{\theta} \mathcal{L}_{LDM}(x', \theta)$ 
7:   end for
8:   for  $k$  from 1 to  $K$  do
9:      $x' \leftarrow x' - \alpha \nabla_{x'} J$ 
10:     $x' \leftarrow \text{clip}(x', x - \zeta, x + \zeta)$ 
11:     $x' \leftarrow \text{clip}(x', 0, 255)$ 
12:   end for
13: end for

```

of the target image used in Liang & Wu (2023) produces a pattern \mathcal{T} with alternate positive and negative pixels, which results in chaotic texture in output images. We then select this latent representation as our \mathcal{T} in Equation 12, as visualized in Figure 5. We also explore different choices of targets in Appendix A.2.

4.3. Implementation

ACE combines the objective function in Equation 12 and the selected pattern. We include finetuning steps in the attack following ASPL (Van Le et al., 2023), but with only a few steps (5 steps for each iteration). This is to strengthen ϵ_{adv} in finetuning. Implementation details are given in Appendix B.

Moreover, we try a fused attack of Equation 12 and the objective function used in PhotoGuard (Salman et al., 2023) and Mist (Liang & Wu, 2023). The target is selected as that in

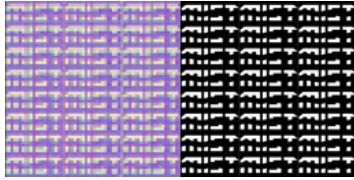


Figure 5. Target \mathcal{T} (left) and its corresponding image (right)

Mist (Liang & Wu, 2023), the same as the image which provides the target for ACE (See in Figure 9). We denote this method as ACE+ and formulate its objective function in Equation 16. The algorithm of ACE/ACE+ is given in Algorithm 1.

$$\begin{aligned}
 & \min_{x'} \mathbb{E}_t \mathbb{E}_{z'(t)|z'(0)} \|s_{\theta}(z'(t), t) - \mathcal{T}\|_2^2 + \alpha \|z'(0) - \mathcal{T}\|_2^2 \\
 & \text{where } z'(0) = \mathcal{E}(x'), \|x' - x\| \leq \zeta
 \end{aligned}
 \tag{16}$$

5. Experiment

We evaluate ACE/ACE+ on two state-of-the-art few-shot generation pipelines empowered by LDM.

LoRA (Hu et al., 2021; Ruiz et al., 2023): The state-of-the-art few-shot generation pipeline. LoRA finetunes the LDM with low-ranked adapters on dozens input images. LoRA generates high-quality images with similar semantic contents to the input images, which raises the concern of

unauthorized artwork style mimicry.

SDEdit (Meng et al., 2021): An image-to-image pipeline that modifies the content of one single image. SDEdit can be used for malicious image faking.

5.1. Experimental Setups

LoRA & Metrics LoRA generates output images with the same semantic contents of input images. As visualized in Figure 6, existing adversarial attacks disturb LoRA mainly by degrading the quality of output images. Hence, we benchmark the performance of adversarial attacks by assessing the quality of LoRA output images.

We finetunes LDM with LoRA and then use the finetuned LDM to generate output images. Finetuning is done on 20 input images with the same content or style. We generate 100 output images with the finetuned LDM and assess their image quality with CLIP-IQA (Wang et al., 2023a), a CLIP-based image quality assessment metric. A high CLIP-IQA score indicates low image quality and strong performance of adversarial attacks. The implementation details of LoRA and CLIP-IQA are discussed in Appendix B.

SDEdit & Metrics SDEdit generates an output image based on an input image, withholding the *structural similarity*. This means that the output and input image are supposed to share the same composition (i.e. the arrangement of elements) and differ mainly in styles and some details. Successful adversarial attacks destroy this structural similarity. Hence, we adopt Multi-Scale SSIM (MS-SSIM) (Wang et al., 2003) and CLIP Image-to-Image Similarity (denoted as CLIP-SIM) (Wang et al., 2023a), two measurements of image-to-image structural similarity, to benchmark how adversarial attacks interfere the structural similarity. A strong adversarial attack is expected to have both these similarity metrics low. Implementation details of SDEdit and two metrics are given in Appendix B.

Datasets & Backbone Model The experiment is conducted on CelebA-HQ (Karras et al., 2017) and Wikiart (Saleh & Elgammal, 2015). For CelebA-HQ, we select 100 images and each of 20 photos describe one identical person. For Wikiart, we select 100 paintings that each of 20 paintings

	CELEBA-HQ			WIKIART		
	SDEdit		LoRA	SDEdit		LoRA
	MS-SSIM ↓	CLIP-SIM ↓	CLIP-IQA ↑	MS-SSIM ↓	CLIP-SIM ↓	CLIP-IQA ↑
NO ATTACK	0.88	93.38	20.66	0.62	89.77	22.88
PHOTOGUARD	0.86	89.24	27.52	0.62	88.01	37.52
PHOTOGUARD+	0.82	91.00	22.91	0.57	89.80	32.62
AdvDM	0.81	83.41	24.53	0.30	85.29	34.03
ASPL	0.82	84.12	<u>33.62</u>	0.30	87.25	<u>46.74</u>
ACE	<u>0.73</u>	<u>74.70</u>	31.46	0.23	76.13	40.54
ACE+	0.69	67.47	35.68	<u>0.29</u>	<u>76.07</u>	48.53

Table 1. Comparison of baseline methods and ours over two few-shot generation pipelines

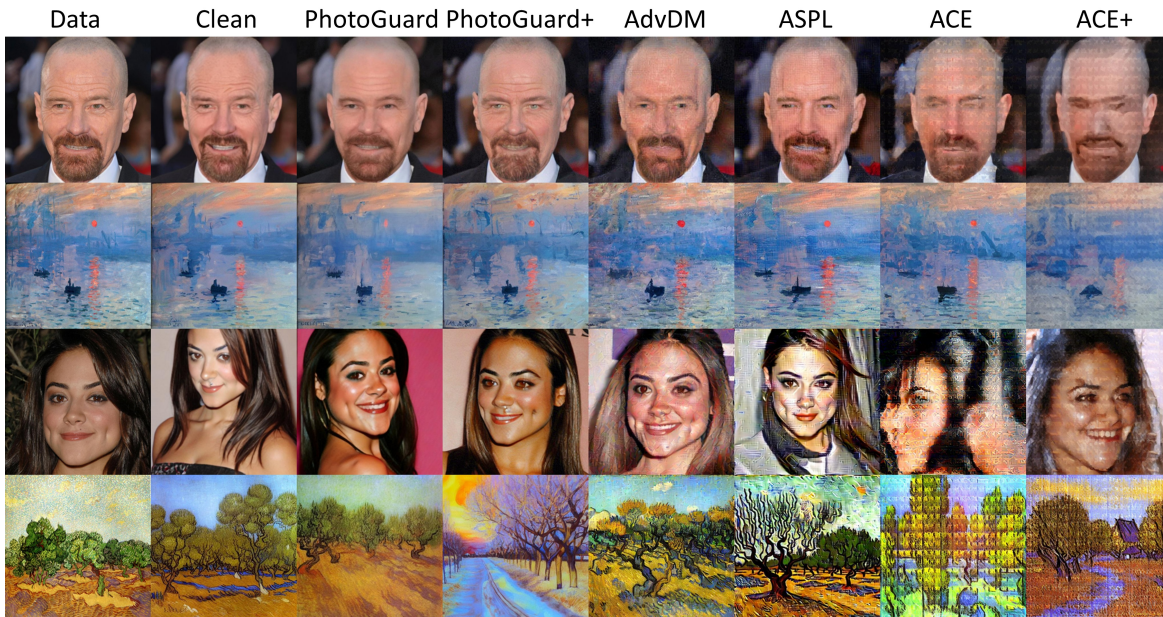


Figure 6. Output images of SDEdit (top two rows) and LoRA (bottom two rows) under different attacks. The adversarial budget is 4/255.

come from the same artist. We use Stable Diffusion 1.5 as the backbone model for attacks, since it has the most active community in few-shot generation among all LDM-based generative models. Additionally, we also investigate the cross-model transferability of ACE/ACE+ with Stable Diffusion 1.4 and Stable Diffusion 2.1 in Section 5.3.

Baselines We compare ACE/ACE+ with existing methods on LDM, including AdvDM (Liang et al., 2023), Encoder Attack and Diffusion Attack in PhotoGuard (Salman et al., 2023), and ASPL (Anti-DreamBooth) (Van Le et al., 2023). Encoder Attack and Diffusion Attack in PhotoGuard (Salman et al., 2023) are denoted by PhotoGuard and PhotoGuard+, respectively. The implementation of baselines is detailed in Appendix B.

Hyperparameters & Implementation Details The adversarial budget ζ in all adversarial attacks is set as 4/255, which is very tiny and acceptable in practice. We

use PGD (Madry et al., 2017) as the optimization for ACE/ACE+, with step length 5×10^{-3} and iteration number 50. We adopt LoRA as the finetuning method used in ACE/ACE+. For ACE+, the loss weight α is set to be 10^2 empirically. LoRA is done for 5 iterations while each iteration finetunes 10 steps. The learning rate is 10^{-5} . All experiments except PhotoGaurd+ are done on one NVIDIA RTX 4090 GPU. The implementation of PhotoGaurd+ is done on one NVIDIA RTX A100 GPU.

5.2. Overall Result

We compare ACE/ACE+ to existing adversarial attacks on LDM. The overall result of comparison are demonstrated in Table 1, where ACE/ACE+ outperform all baseline methods in disturbing SDEdit and LoRA. Figure 6 visualizes cases of output images of LoRA and SDEdit under baseline methods and ACE/ACE+. More visualization is given in Appendix C.

VICTIM	SD1.4			SD1.5			SD2.1		
BACKBONE	SDEdit		LoRA	SDEdit		LoRA	SDEdit		LoRA
	MS ↓	CS ↓	CI ↑	MS ↓	CS ↓	CI ↑	MS ↓	CS ↓	CI ↑
NO ATTACK	0.85	91.71	20.32	0.85	91.16	19.22	0.80	79.00	16.78
SD1.4	0.73	77.24	38.13	0.73	77.58	35.98	0.62	60.82	35.45
SD1.5	0.73	77.29	36.65	0.73	77.50	32.11	0.72	60.10	45.05
SD2.1	0.72	76.20	46.08	0.62	76.80	39.08	0.60	59.12	43.89

VICTIM	SD1.4			SD1.5			SD2.1		
BACKBONE	SDEdit		LoRA	SDEdit		LoRA	SDEdit		LoRA
	MS ↓	CS ↓	CI ↑	MS ↓	CS ↓	CI ↑	MS ↓	CS ↓	CI ↑
NO ATTACK	0.85	91.71	20.32	0.85	91.16	19.22	0.80	79.00	16.78
SD1.4	0.67	66.83	40.69	0.67	66.40	31.53	0.58	56.41	67.96
SD1.5	0.67	66.58	41.16	0.67	66.13	36.05	0.58	57.17	68.50
SD2.1	0.67	66.33	41.80	0.67	57.17	41.96	0.58	57.27	73.59

Table 2. Cross-model transferability of ACE(top) and ACE+(bottom). MS, CS, and CI are our three metrics, MS-SSIM, CLIP-SIM, and CLIP-IQA, for short, respectively.

One important observation is that the chaotic texture on the output images of ACE/ACE+ show patterns consistent with those in Figure 3. This indicates the flexibility of ACE/ACE+ that they make the pattern of the texture optimizable. We believe that there are targets that yield better performance than our used target, which can be found through optimization. We omit this to future works.

Another observation is that although output images under ACE/ACE+ are visibly filled with chaotic texture, their advantage in quantitative indicators is not obvious (See in Figure 6 and Appendix C). This may be caused by the inconsistency between machine and human vision on *what the image with the worst quality is like*. Model-based measurements are trained to fit human’s preference on what good images are like. It is natural that they perform differently from human in determining what bad images are like. Hence, we believe the visualization may be a necessary view to benchmark adversarial attacks on LDM.

5.3. Cross-model Transferability

Adversarial attacks on LDM are white-box and model-dependent. In this part, we investigate how ACE/ACE+ perform on other LDM-based text-guided generative models, which impacts the practicality of the attack.

We evaluate this cross-model transferability on three LDM-based text-guided generative models: Stable Diffusion 1.4, Stable Diffusion 1.5, and Stable Diffusion 2.1. Details of implementation are given in Appendix B. In our experiment, *backbone* means the model used to generate adversarial examples and *victim* means the model used for few-shot generation.

We use 100 images from CelebA-HQ, 20 in each of 5 groups, to generate adversarial examples on three backbone models and run SDEdit and LoRA with these adversarial examples

on three victim models. Experimental setups stay the same with those stated in Section 5.1, except for increasing the strength of SDEdit to 0.4 to boost the diversity of output images for better visualization. Table 2 demonstrates the result that ACE/ACE+ can disturb few-shot generation of LDM-based text-guided image generative models even the victim is different than the backbone. Visualized results are given in Appendix C.4

5.4. Additional Results

In addition to the performance, we conduct experiments to investigate the following problems. Due to the space limit, we omit their results to the appendix.

- Memory efficiency improvements of ACE/ACE+ and memory efficiency comparison between ACE/ACE+ and existing adversarial attacks (Appendix A.1).
- How different choices of target \mathcal{T} influence the performance of ACE/ACE+ (Appendix A.2).
- How ACE/ACE+ survive denoising methods, the most straight-forward counteraction of adversarial attacks on LDM (Appendix A.3).

6. Conclusion

In this paper, we reveal the dynamics why adversarial attacks on LDM work successfully in disturbing the finetuning of LDM. Based on the dynamics, we propose ACE, an improved method for adversarial attacks on LDM, which achieves state-of-the-art performance. ACE can serve as a practical tool to protect personal images from being used in unauthorized few-shot generation empowered by LDM. Our work shows the potential to further improve adversarial attacks on LDM by optimizing the target.

References

- Anderson, B. D. Reverse-time diffusion equation models. *Stochastic Processes and their Applications*, 12(3):313–326, 1982.
- Carlini, N. and Wagner, D. Towards evaluating the robustness of neural networks. In *2017 IEEE Symposium on Security and Privacy (SP)*, pp. 39–57. Ieee, 2017.
- Chen, C., Fu, J., and Lyu, L. A pathway towards responsible ai generated content. *arXiv preprint arXiv:2303.01325*, 2023.
- Chen, T., Xu, B., Zhang, C., and Guestrin, C. Training deep nets with sublinear memory cost. *arXiv preprint arXiv:1604.06174*, 2016.
- Das, N., Shanbhogue, M., Chen, S.-T., Hohman, F., Li, S., Chen, L., Kounavis, M. E., and Chau, D. H. Shield: Fast, practical defense and vaccination for deep learning using jpeg compression. In *Proceedings of the 24th ACM SIGKDD International Conference on Knowledge Discovery & Data Mining*, pp. 196–204, 2018.
- Devlin, J., Chang, M.-W., Lee, K., and Toutanova, K. Bert: Pre-training of deep bidirectional transformers for language understanding. *arXiv preprint arXiv:1810.04805*, 2018.
- Esser, P., Rombach, R., and Ommer, B. Taming transformers for high-resolution image synthesis. In *Proceedings of the IEEE/CVF conference on computer vision and pattern recognition*, pp. 12873–12883, 2021.
- Fan, M., Chen, C., Wang, C., and Huang, J. On the trustworthiness landscape of state-of-the-art generative models: A comprehensive survey. *arXiv preprint arXiv:2307.16680*, 2023.
- Gal, R., Alaluf, Y., Atzmon, Y., Patashnik, O., Bermano, A. H., Chechik, G., and Cohen-Or, D. An image is worth one word: Personalizing text-to-image generation using textual inversion. *arXiv preprint arXiv:2208.01618*, 2022.
- Goodfellow, I. J., Shlens, J., and Szegedy, C. Explaining and harnessing adversarial examples. *arXiv preprint arXiv:1412.6572*, 2014.
- Ho, J., Jain, A., and Abbeel, P. Denoising diffusion probabilistic models. *Advances in neural information processing systems*, 33:6840–6851, 2020.
- Hu, E. J., Shen, Y., Wallis, P., Allen-Zhu, Z., Li, Y., Wang, S., Wang, L., and Chen, W. Lora: Low-rank adaptation of large language models. *arXiv preprint arXiv:2106.09685*, 2021.
- Karras, T., Aila, T., Laine, S., and Lehtinen, J. Progressive growing of gans for improved quality, stability, and variation. *arXiv preprint arXiv:1710.10196*, 2017.
- Lefaudeux, B., Massa, F., Liskovich, D., Xiong, W., Caggiano, V., Naren, S., Xu, M., Hu, J., Tintore, M., Zhang, S., Labatut, P., and Haziza, D. xformers: A modular and hackable transformer modelling library. <https://github.com/facebookresearch/xformers>, 2022.
- Liang, C. and Wu, X. Mist: Towards improved adversarial examples for diffusion models. *arXiv preprint arXiv:2305.12683*, 2023.
- Liang, C., Wu, X., Hua, Y., Zhang, J., Xue, Y., Song, T., Xue, Z., Ma, R., and Guan, H. Adversarial example does good: Preventing painting imitation from diffusion models via adversarial examples. *arXiv preprint arXiv:2302.04578*, 2023.
- Madry, A., Makelov, A., Schmidt, L., Tsipras, D., and Vladu, A. Towards deep learning models resistant to adversarial attacks. *arXiv preprint arXiv:1706.06083*, 2017.
- Meng, C., He, Y., Song, Y., Song, J., Wu, J., Zhu, J.-Y., and Ermon, S. Sdedit: Guided image synthesis and editing with stochastic differential equations. *arXiv preprint arXiv:2108.01073*, 2021.
- Mustafa, A., Khan, S. H., Hayat, M., Shen, J., and Shao, L. Image super-resolution as a defense against adversarial attacks. *IEEE Transactions on Image Processing*, 29: 1711–1724, 2019.
- Podell, D., English, Z., Lacey, K., Blattmann, A., Dockhorn, T., Müller, J., Penna, J., and Rombach, R. Sdxl: improving latent diffusion models for high-resolution image synthesis. *arXiv preprint arXiv:2307.01952*, 2023.
- Radford, A., Kim, J. W., Hallacy, C., Ramesh, A., Goh, G., Agarwal, S., Sastry, G., Askell, A., Mishkin, P., Clark, J., et al. Learning transferable visual models from natural language supervision. In *International conference on machine learning*, pp. 8748–8763. PMLR, 2021.
- Rombach, R., Blattmann, A., Lorenz, D., Esser, P., and Ommer, B. High-resolution image synthesis with latent diffusion models. In *Proceedings of the IEEE/CVF conference on computer vision and pattern recognition*, pp. 10684–10695, 2022.
- Ruiz, N., Li, Y., Jampani, V., Pritch, Y., Rubinstein, M., and Aberman, K. Dreambooth: Fine tuning text-to-image diffusion models for subject-driven generation. In *Proceedings of the IEEE/CVF Conference on Computer Vision and Pattern Recognition*, pp. 22500–22510, 2023.

- Saleh, B. and Elgammal, A. Large-scale classification of fine-art paintings: Learning the right metric on the right feature. [arXiv preprint arXiv:1505.00855](#), 2015.
- Salman, H., Khaddaj, A., Leclerc, G., Ilyas, A., and Madry, A. Raising the cost of malicious ai-powered image editing. [arXiv preprint arXiv:2302.06588](#), 2023.
- Shan, S., Cryan, J., Wenger, E., Zheng, H., Hanocka, R., and Zhao, B. Y. Glaze: Protecting artists from style mimicry by text-to-image models. [arXiv preprint arXiv:2302.04222](#), 2023a.
- Shan, S., Ding, W., Passananti, J., Zheng, H., and Zhao, B. Y. Prompt-specific poisoning attacks on text-to-image generative models. [arXiv preprint arXiv:2310.13828](#), 2023b.
- Sohl-Dickstein, J., Weiss, E., Maheswaranathan, N., and Ganguli, S. Deep unsupervised learning using nonequilibrium thermodynamics. In [International conference on machine learning](#), pp. 2256–2265. PMLR, 2015.
- Song, Y. and Ermon, S. Generative modeling by estimating gradients of the data distribution. [Advances in neural information processing systems](#), 32, 2019.
- Song, Y., Sohl-Dickstein, J., Kingma, D. P., Kumar, A., Ermon, S., and Poole, B. Score-based generative modeling through stochastic differential equations. [arXiv preprint arXiv:2011.13456](#), 2020.
- Szegedy, C., Zaremba, W., Sutskever, I., Bruna, J., Erhan, D., Goodfellow, I., and Fergus, R. Intriguing properties of neural networks. [arXiv preprint arXiv:1312.6199](#), 2013.
- Van Le, T., Phung, H., Nguyen, T. H., Dao, Q., Tran, N., and Tran, A. Anti-dreambooth: Protecting users from personalized text-to-image synthesis. [arXiv preprint arXiv:2303.15433](#), 2023.
- Wang, J., Chan, K. C., and Loy, C. C. Exploring clip for assessing the look and feel of images. In [Proceedings of the AAAI Conference on Artificial Intelligence](#), volume 37, pp. 2555–2563, 2023a.
- Wang, T., Zhang, Y., Qi, S., Zhao, R., Xia, Z., and Weng, J. Security and privacy on generative data in aigc: A survey. [arXiv preprint arXiv:2309.09435](#), 2023b.
- Wang, Z., Simoncelli, E. P., and Bovik, A. C. Multi-scale structural similarity for image quality assessment. In [The Thirty-Seventh Asilomar Conference on Signals, Systems & Computers, 2003](#), volume 2, pp. 1398–1402. Ieee, 2003.
- Xie, C., Wang, J., Zhang, Z., Ren, Z., and Yuille, A. Mitigating adversarial effects through randomization. [arXiv preprint arXiv:1711.01991](#), 2017.
- Xue, H., Liang, C., Wu, X., and Chen, Y. Toward effective protection against diffusion based mimicry through score distillation. [arXiv preprint arXiv:2311.12832](#), 2023.
- Ye, H., Zhang, J., Liu, S., Han, X., and Yang, W. Ip-adapter: Text compatible image prompt adapter for text-to-image diffusion models. [arXiv preprint arXiv:2308.06721](#), 2023.
- Zantedeschi, V., Nicolae, M.-I., and Rawat, A. Efficient defenses against adversarial attacks. In [Proceedings of the 10th ACM Workshop on Artificial Intelligence and Security](#), pp. 39–49, 2017.
- Zhao, Z., Duan, J., Hu, X., Xu, K., Wang, C., Zhang, R., Du, Z., Guo, Q., and Chen, Y. Unlearnable examples for diffusion models: Protect data from unauthorized exploitation. [arXiv preprint arXiv:2306.01902](#), 2023.

A. Additional Experiments

A.1. Memory Efficiency

A.1.1. MEMORY EFFICIENCY OF ACE/ACE+

Memory efficiency is crucial for adversarial attacks on LDM, because the main body of their users are non-developers who do not have access to GPUs with large VRAM. Hence, we also work on improving the memory efficiency of ACE/ACE+. The memory cost of ACE/ACE+ consists of three occupies, which store model weights, the computational graph, and the optimizer states, respectively. In the adversarial attack, we only optimize the inputs so the memory used to store optimizer states is small. We save memory cost mainly by decreasing the memory to store model weights and computational graph. Following toolkit and mechanisms are introduced to the implementation of our attack.

xFormers We leverage xFormers (Lefaudeux et al., 2022) to reduce the memory cost used to store the computational graph. xFormers is a toolbox that provides memory-efficient computation operators for training and inference of transformer-based modules. We use their attention operator in the computation of cross attention layers of UNet in LDM when computing gradients.

Gradient Checkpointing (Chen et al., 2016) A common tool of memory-efficient training is Gradient Checkpointing. Gradient Checkpointing separates a neural network into blocks. In forward-propagation, it only stores the activation. The back-propagation is done block by block. For each block, it reconstructs the forward computational graph within the block with the stored activation. Then, it constructs the backward computational graph within the block and compute the gradient over the activation. This greatly reduces the GPU memory at the cost of computing time. To balance the memory and time cost, we only apply gradient checkpointing in the down-block, mid-block, and up-block of the UNet.

A.1.2. EVALUATION

We evaluate the GPU memory cost of existing adversarial attacks on LDM and that of our attack. The setup of these baseline attacks and ours stay the same as that in Section 5.1. The result in Figure 7 shows that the GPU memory cost of ACE/ACE+ outperforms all baseline attacks.

We highlight that our GPU memory cost is lower than 6GB. This means that **ACE/ACE+ is able to run on most of the consumer-level GPUs**. This helps popularize the application of adversarial attacks on LDM as a practical tool.

One concern of our memory-efficient attack is about the time cost. We also evaluate the running time of attacking 20 images with our attack, which is 1739 seconds on one NVIDIA RTX 4090 GPU. This running time is acceptable for users who protect their personal images since the sum of these images may not be large.

Method	Memory/GB
PhotoGuard	6.16
PhotoGuard+	16.79
AdvDM	6.28
Anti-DB	7.33
ACE&ACE+	5.77

Figure 7. VRAM cost of our method and baselines

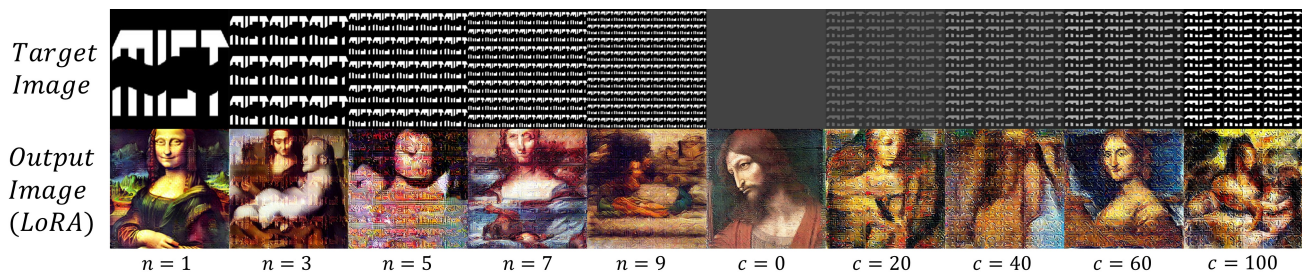


Figure 8. Target images with different pattern repetition and contrast results in different effects.

A.2. Different Targets

The target \mathcal{T} is an important parameter of ACE/ACE+. In our experiments, we select \mathcal{T} as the latent representation $z(0)$ of the image used in Liang & Wu (2023). We demonstrate the image and the latent representation in Figure 5. Additionally, we also explore the effectiveness of different targets in ACE/ACE+. The results validate our choice of the target.

First, we try to use the latent representation of natural images as the target \mathcal{T} . This follows the advice of Van Le et al. (2023). We apply ACE/ACE+ with the target and visualize the output images of the victim LoRA in Figure 9. It shows that the latent representation of natural images add minor noise to the output image but cannot yield satisfying results in disturbing LoRA. **This indicates that both the objective function and our choice of the target \mathcal{T} are the key.**

Second, we investigate the impact of two vision variables in the target image \mathcal{T} : pattern density and contrast. The setup follows that in the first experiment above. The result is visualized in Figure 8. When the pattern is sparse, increasing pattern density yields better attacking performance. When the pattern is dense, increasing pattern density then leads to worse performance. Hence, in practice, we choose an appropriate pattern density. As for contrast, the performance of the attack increases as the pattern’s contrast goes higher. We then let our target be with the highest contrast.



Figure 9. Comparison to trivial target images.

A.3. ACE vs Denoising Methods

DEFENSE	NO DEFENSE	GAUSSIAN		JPEG		RESIZING		SR
PARAMS		$\sigma = 4$	$\sigma = 8$	$Q = 20$	$Q = 70$	2x	0.5x	
LoRA	25.51	17.24	28.39	38.13	29.01	26.10	32.91	39.63
SDEdit	0.54	0.70	0.64	0.75	0.75	0.79	0.76	0.45

Table 3. Performance under different anti-attack methods. The noise budget is set to 8/255

We conduct an experiment to investigate how our attacks survive denoising methods, the most straight-forward way to counter adversarial attacks on LDM in practice. We use ACE/ACE+ to generate adversarial examples from one 20-image group from CelebA-HQ. Then, we use several common denoising methods to denoise the adversarial perturbations on the examples. After that, we apply SDEdit and LoRA on these purified adversarial examples. The experimental setup follows the setup in Section 5.1 except for the adversarial perturbation constraint, which is set to be 8/255. This is still a small constraint compared to the setup of existing adversarial attacks (For comparison, Salman et al. (2023) and Van Le et al. (2023) use 16/255). The denoising methods include Gaussian (Zantedeschi et al., 2017), JPEG (Das et al., 2018), Resizing (Xie et al., 2017), SR (Mustafa et al., 2019). Specifically, Gaussian adds Gaussian noise of standard variance 4 and 8 to the adversarial example. We try two JPEG compression qualities, 20 and 70. For Resizing we have two setups, 2x up-scaling + recovering (denoted by 2x) and 0.5x down-scaling + recovering (denoted by 0.5x). The interpolation algorithm in resizing is bicubic.

The quantitative result is demonstrated in Table 3. It shows that ACE and ACE+ still have strong impact on the output image quality of LDM-driven few-shot generation after processing by denoising-based adversarial defense. The CLIPQA score of most cases even increase after the adversarial defense. Hence, we believe that our adversarial attack has enough robustness to denoising-based adversarial defense.

Table 4 visualizes the output images of SDEdit and LoRA referring to the adversarial examples which are processed by different denoising-based adversarial defense methods. For both method, they still have strong performance under most of the cases except for Gaussian Noise($\sigma = 8$) and JPEG compression (quality= 20). However, in the exception cases, the defense has added visible degradation to the image, which also heavily affect both LoRA and SDEdit process. For example, LoRA learns to produce images comprised of small squares due to a hard compression of quality 20. And SDEdit produces images of visible Gaussian noise when adding Gaussian noise of $\sigma = 8$ as defense. It’s noteworthy that both ACE and ACE+ seems to be strengthened after SR defense, which is an intriguing phenomena.

A.4. Different Prompts in LoRA Training

In real life usage, malicious ones may use different prompts to finetune the LDM. Hence, we investigate whether ACE maintains effectiveness under different prompts in the finetuning. We select one 20-image group from CelebA-HQ and use ACE to generate adversarial examples under adversarial budget 4/255 and prompt *a photo of a sks person*. We then train LoRA with four different prompts:

Improving Adversarial Attacks on Latent Diffusion Model

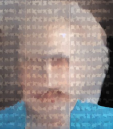
DEFENSE	NO DEFENSE	GAUSSIAN		JPEG		RESIZING		SR
PARAMS		$\sigma = 4$	$\sigma = 8$	$Q = 20$	$Q = 70$	2x	0.5x	
LoRA								
SDEdit								

Table 4. Performance under different denoising methods. The noise budget is set to 8/255

- a photo of a sks person
- a photo of a **pkp**
- a photo of a **pkp woman**
- **an image of a pkp woman**

We visualize the output images in Table 5. The result shows minor degradation in the effectiveness of attack when ACE handles more and more unfamiliar prompts. However, there still exists strong visual distortion under all three unknown prompts.

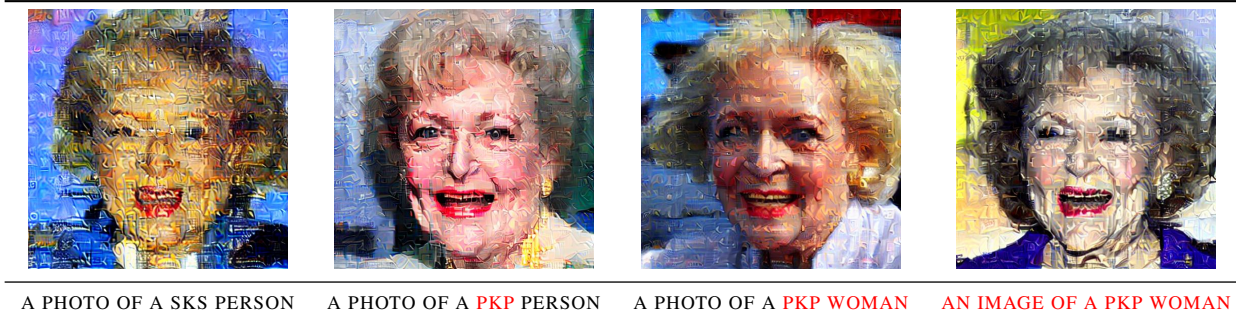


Table 5. LoRA output images with different prompts under the attack of ACE. Red text notes the difference between the prompt in generation and the prompt in finetuning.

A.5. Details of Validation Experiments

A.5.1. COMPUTATION OF COSINE SIMILARITY

We compute cosine similarity of $B_{spl}, B_x(t)$ with ϵ_{adv} in Section 3.2 and Section 4.1. Given two set of images A, B for calculation, we first calculate the metric (for example B_{spl}) for each $a \in A, b \in B$. Then we calculate the cosine similarity for every $(a, b) \in A \times B$. We take the average of the results as our final answer.

A.5.2. VISUALIZATION OF VARIABLES IN THE LATENT SPACE OF LDM

We describe how to visualize variables in the latent space of LDM, including $\epsilon_{adv}, B_x,$ and B_{spl} . These variables are of size $64 \times 64 \times 4$. Given a variable $E \in \mathbb{R}^{64 \times 64 \times 4}$, we first do normalization by $E' = \frac{E - \min(E)}{\max(E) - \min(E)}$. After the normalization, we directly plot E' as a heatmap. The used color bar is demonstrate in Figure 10.

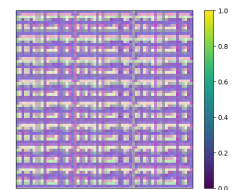


Figure 10. An example for visualization. We use the same color bar in all visualizations.

B. Implementation and Experimental Details

LoRA For the evaluation, we finetune LDM with on CelebA-HQ dataset using the prompt *a photo of a sks person*, which was first used in the paper of Anti-Dreambooth (Van Le et al., 2023). This is because CelebA-HQ consists of portraits of certain people. Similarly, we use the prompt *a photo of a sks painting* on the WikiArt dataset, because WikiArt consists of paintings by certain artists. The number of finetuning epochs is set to be 1000 which ensures LoRA on clean images achieves considerate performance.

SDEdit The strength of SDEdit is set to be 0.3, which makes sense because a higher strength modifies the input image too much and a lower one keeps too many details of the input image. We use a null prompt to avoid the effect of prompts in the generation.

Metrics For MS-SSIM, we use the default setting in the implementation¹. CLIP-SIM computes the cosine similarity between the input images and the output images in the semantic space of CLIP (Radford et al., 2021) and is given by the following definition:

$$\text{CLIP-SIM}(X, Y) = \cos(\mathcal{E}_{clip}(X), \mathcal{E}_{clip}(Y)) \quad (17)$$

where \mathcal{E}_{clip} is the vision encoder of the CLIP (Radford et al., 2021) model. CLIP-IQA is a non-reference image quality assessment metric that computes the text-image similarity between the image and some positive & negative prompts. In the official implementation², the author exploits prompts such as *Good image*, *Bad image*, and *Sharp image*. An image with high quality is expected to have high text-image similarity with positive prompts and low text-image similarity with negative prompts. In our experiments, we use the positive prompt *A good photo of a person* and the negative prompt *A bad photo of a person* for CelebA-HQ and the positive prompt *A good photo of a painting* and the negative prompt *A bad photo of a painting* for WikiArt. Since we want to measure how poor the output image quality is, we use the text-image similarity between output images and the negative prompt. A strong adversarial attack results in low quality of output images and a high similarity between output images and the negative prompt.

Image Resolution The standard resolution for SD1.x is 512, while the one for SD2.x is 768. For cross-model transferability experiments, we set the resolution of every model to 512, disregarding that the standard resolution of SD2.1 is 768. The reason for this uniform resolution is to avoid the resizing, which may introduce distortion to the attacks. However, as LoRA on SD2.1 naturally generate image of resolution 768, we still test LoRA performance on SD2.1 on resolution 768.

Baselines We use the official implementation of PhotoGuard³, PhotoGuard+⁴, AdvDM⁵, and Anti-Dreambooth⁶ in our experiments. For PhotoGuard and PhotoGuard+, we follow the default setup in the official Python implementation file^{7 8}, except for tuning the adversarial budget to $4/255$. We also set the surrogate model of PhotoGuard to be Stable Diffusion v1.5. PhotoGuard+ aims to attack an inpainting task, and we simply set the inpainting mask to 1 for all pixels, as both SDEdit and LoRA operates on full pixels. For AdvDM, we also follow the default setup in the official implementation. For Anti-Dreambooth, we directly use the official implementation except for transferring it to LoRA. The default setup sets 10 steps of training LoRA and 10 steps of PGD attacks in every epoch. However, the default epochs of Anti-Dreambooth is too time-consuming. Therefore, we tune the total epochs of one single attack to be 4, which is a fair comparison for our method.

C. Visualization

In this section, we visualize the comparison result between our proposed methods, ACE and ACE+, and baseline methods.

C.1. Adversarial Examples

Figure 11 demonstrates adversarial examples generated by our adversarial attack, which resembles a real image since the adversarial budget $\zeta = 4/255$ is quite small.

¹<https://github.com/VainF/pytorch-msssim>

²<https://github.com/IceClear/CLIP-IQA>

³<https://github.com/MadryLab/photoguard>

⁴<https://github.com/MadryLab/photoguard>

⁵<https://github.com/mist-project/mist>

⁶<https://github.com/VinAIRresearch/Anti-DreamBooth>

⁷https://github.com/MadryLab/photoguard/blob/main/notebooks/demo_simple_attack_inpainting.ipynb

⁸https://github.com/MadryLab/photoguard/blob/main/notebooks/demo_complex_attack_inpainting.ipynb

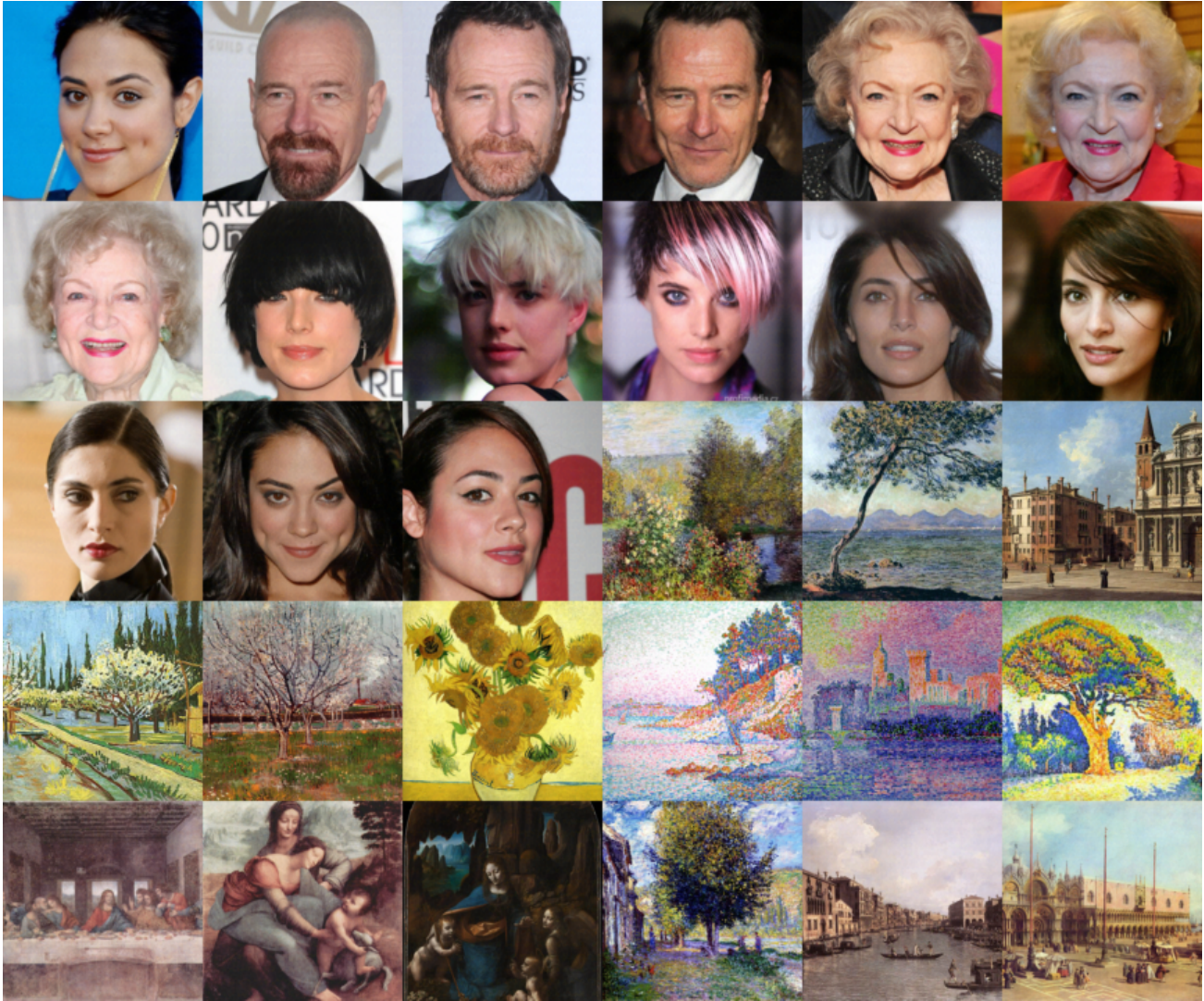


Figure 11. Adversarial examples on LDM generated by our proposed method with the adversarial perturbation budget $\zeta = 4/255$. The perturbation is quite small and almost human-invisible, making the adversarial examples resemble real examples.

C.2. Output images of SDEdit

Figure 12 visualizes the output images of SDEdit under different adversarial attacks. All adversarial attacks are budgeted by $\zeta = 4/255$. Two proposed methods add obvious noise to the output image, compared to no attack and three baseline methods, Photoguard, AdvDM, and Anti-DB. Note that the texture in the output images of ACE/ACE+ shows consistency with the pattern demonstrated in Figure 3.

C.3. Output images of LoRA

Figure 13, 14, 15, and 16 show the output images of LoRA under different adversarial attacks. All adversarial attacks are budgeted by $\zeta = 4/255$. Note that the texture in the output images of ACE/ACE+ shows consistency with the pattern of the sampling bias \mathcal{B}_{spl} demonstrated in Figure 3. It is naturally because the texture is caused by the sampling error, which is accumulated by \mathcal{B}_{spl} .

C.4. Cross-model Transferability

We visualize the output images of different victim models under ACE by different backbone models in Table 6. As shown in the table, our method shows a strong consistency among different models. An exception is that when using SD2.1 as the victim model, it tends to fail in LoRA training(not learning the right person) instead of learning the strong semantic distortion from the target image. However, the model does learn the right person when no attack is conducted. Also, the SDEdit process is extra strong when victim is SD2.1. We attribute this phenomena to the resolution mismatch. SD2.1 is trained to receive images of resolution 768, while we actually fed it with images of resolution 512. This may leads to different behaviour of SD2.1. Also, the resolution mismatch between SD1.x and SD2.x may be the main reason for the performance degradation when using SD1.x as victim and SD2.1 as backbone.

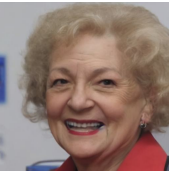
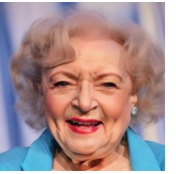
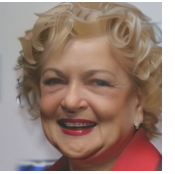
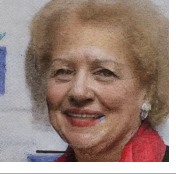
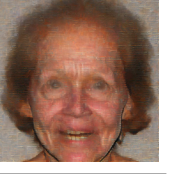
VICTIM	SD1.4		SD1.5		SD2.1	
BACKBONE	SDEdit	LoRA	SDEdit	LoRA	SDEdit	LoRA
NO ATTACK						
SD1.4						
SD1.5						
SD2.1						

Table 6. Visualization of cross-model transferability of ACE.

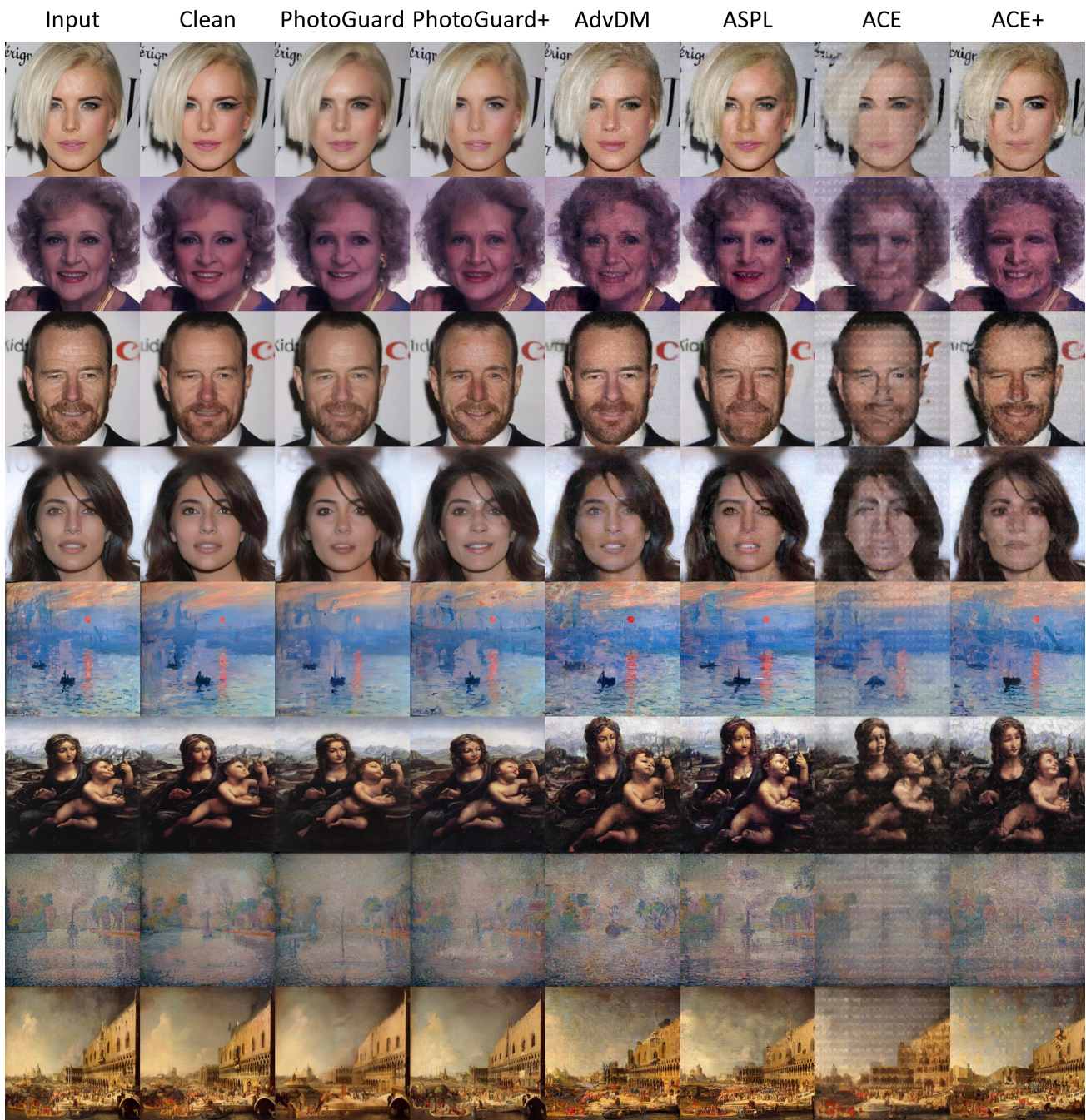


Figure 12. Output images of SDEdit under different adversarial attacks. With the same perturbation budget, our attacks better interfere the image quality compared to three baseline methods. Specifically, ACE adds chaotic texture to the image. ACE erases some contents of the image.



Figure 13. Output images of LoRA under different adversarial attacks. Two proposed methods outperform baseline methods.

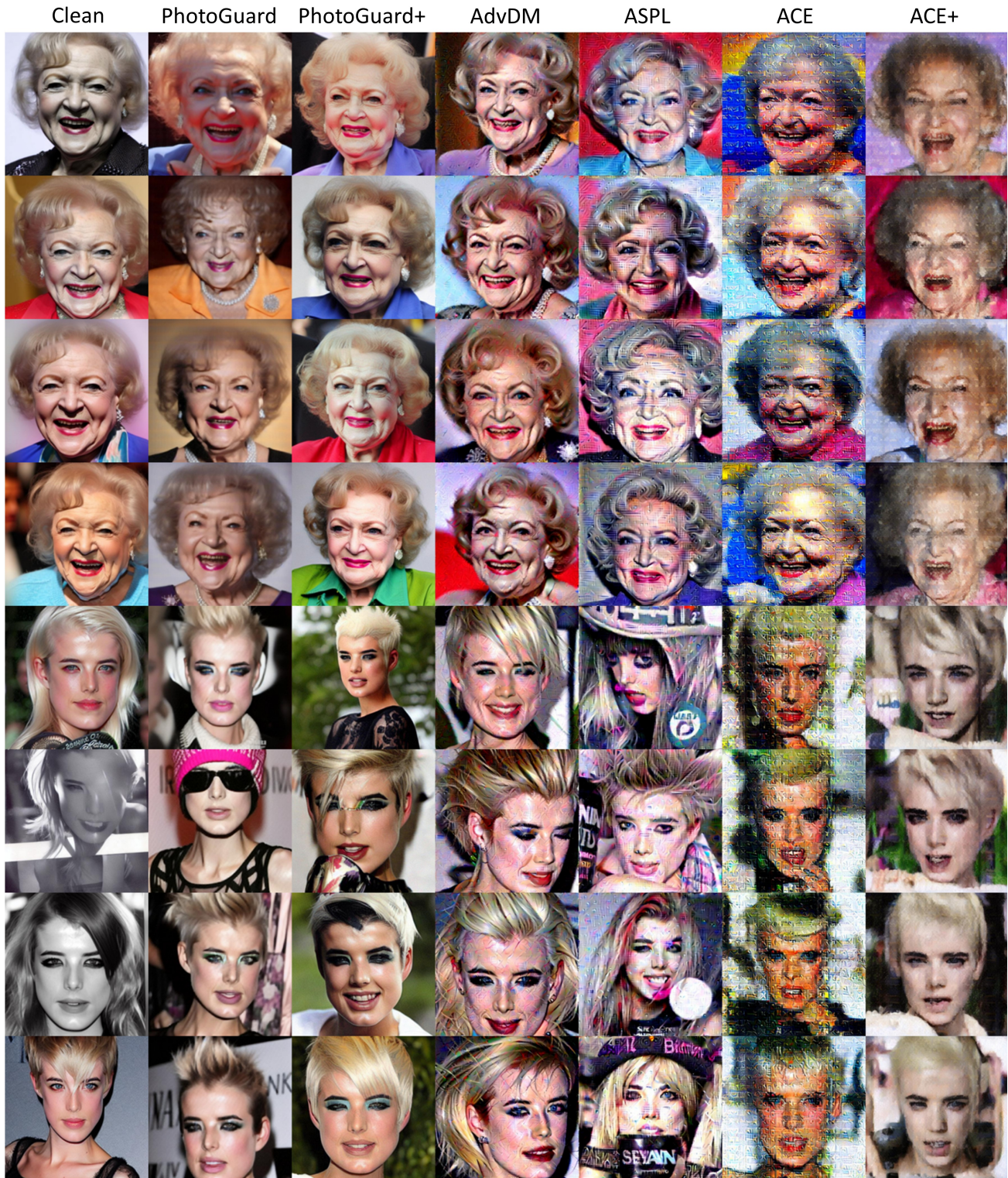


Figure 14. Output images of LoRA under different adversarial attacks. ACE and ACE+ outperform baseline methods. (Cont.)



Figure 15. Output images of LoRA under different adversarial attacks. ACE and ACE+ outperform baseline methods. (Cont.)



Figure 16. Output images of LoRA under different adversarial attacks. ACE and ACE+ outperform baseline methods. (Cond.)